COMPARISON AND EFFECTIVENESS OF SLIP MODE FREQUENCY SHIFT AND SANDIA FREQUENCY SHIFT ACTIVE METHODS FOR ISLANDING DETECTION IN SINGLE-PHASE GRID-CONNECTED PHOTOVOLTAIC SYSTEMS

FADILA BARKAT[1], ALI CHEKNANE[1], JOSEP M. GUERRERO[2], GEORGE CULEA[3], PETRU LIVINTI[3], IOAN VIOREL BANU[3*]

[1] Semiconductors and Functional Material Laboratory, Faculty of Technology, University of Amar Telidji, Laghouat 03000, Algeria
[2] The Villum Center for Research on Microgrids (CROM), AAU Energy, Aalborg University, 9220 Aalborg East, Denmark
[3] "Vasile Alecsandri" University of Bacau, Calea Marasesti 157, Bacau, 600115, Romania
* Correspondence: ibanu86@yahoo.com

Received: date: 13.05.2022
Revised: date: 31.05.2022
Accepted: date: 30.06.2022
Published: date: 26.06.2025

Abstract: This paper offers a comprehensive comparison for the effects of two most important active anti-islanding detection methods which are the slip mode shift frequency (SMS) and Sandia frequency shift (SFS). The comparison is proved in detail through the simulation of the proposed single-phase photovoltaic (PV) system in the Matlab/Simulink. The obtained results show that islanding operation can be successfully detected and prevented using the studied active methods with adequate values for grid power and local load quality factor. In addition, adequate parameters of each method lead to reduce the non-detection zone (NDZ) and prevent the failure of the studied methods.

Keywords: active methods, islanding, inverter, photovoltaic (PV), Sandia frequency shift (SFS), slip mode frequency shift (SMS)

1. INTRODUCTION

Islanding is a phenomenon when a portion of a utility that contains both loads and distributed generation (DG) systems is isolated from the grid and keeps working on. Islanding is generally undesirable due to the fact that it creates a safety hazard to the service personnel or can conduct to asynchronous reclose that can damage the equipment [1]. Because of these risks, utilities and applicable codes and standards such as IEC 62116, IEEE Std. 929, and IEEE Std. 1547 have been established [2]. Effective and reliable anti-islanding detection methods are employed according to the IEEE Std. 929 [1] to deal with islanding operation and propose a procedure for testing the DG and protecting the system.

Passive methods are developed for islanding detection [3]. They are based on the system parameters measurement like under/over voltage (UOV) and under/over frequency (UOF) [4]. The effectiveness of the passive methods depends on the monitoring parameters thresholds to identify the islanding mode. The voltage threshold is between 88% and 110% of nominal value and the frequency threshold is set between 59.3 Hz and 60.5 Hz [1]. The main disadvantage of the passive methods is a large non-detection zone (NDZ) [5] so this later phenomenal effect is not surmounted using passive methods.

* Corresponding author, email: ionut.banu@ub.ro
https://doi.org/10.29081/jesr.v30i4.001

To avoid this situation, active methods have been proposed. These active anti-islanding methods introduce a small perturbation at the point of common coupling (PCC) to minimize the so-called NDZ [5-7]. This domain means islanding phenomenon detection methods, especially active methods, have attracted a lot of research. There are also hybrid islanding methods like [8], [9], and [10] and anti-islanding techniques specially adapted for microgrids [11-14].

NDZ systems were implemented using a rather simple methodology, specifically for passive methods [5]. Reference [15] showed a detailed description of the three common active methods and their NDZ in the load parameter space based on the quality factor (Q_f) versus resonant frequencies (f_0) and evaluated their performance.

The systems based on photovoltaic (PV) sources as current source and grid-connected as voltage source have been a subject of interest for many researchers, but it can adversely affect the effectiveness of the systems by using a complete PV source and boost converter with maximum power point tracking (MPPT) to rise the PV system performance. It has been noted the existence of a few related researches on this domain, however they are limited since they are considering a voltage source in the place of a PV array thus, the effects of radiation and shading are not presented and, without them, the results may be wrong or uncertain.

This paper aims at comparing and evaluating the performance of two common active methods namely Sandia frequency shift (SFS) [6] and slip mode shift frequency (SMS) [16] applied on an effective system under islanding mode to locate their boundaries. These may give appropriate values for detection time and may offer correct boundaries of each method when compared with conventional state. In this study, the SFS and SMS methods are investigated with more details and with different cases to cover all possibilities for each method. The NDZ and quality factor influence of each method are also investigated in this work for different cases. These methods are carried out on a proposed 3.5 kW single-phase grid connected PV system with a DC-AC PV inverter with Perturb and Observe (P&O) MPPT controller [17] and an active anti-islanding detection unit, a 240 V utility grid, and a parallel *RLC* load which has parameters to make the Q_f equals to 2.5 [6, 15]. In this case all parameters are taken according to IEEE Std. 929 and the proposed model designed under the Matlab/Simulink environment is adaptable under other standardizations.

The paper has the following structure. Section 2 presents the studied PV system under islanding, including the implemented simulation model in Matlab/Simulink. Section 3 presents the simulation results. The last section of the paper presents the main conclusions.

The purpose of the paper is to find out which of the two methods is better to use in relation to the detection time, the quality of signal, and the limits of each one of them. Furthermore, this study may provide a broad overview of how these approaches interact with the passive ones, leading to a fresh viewpoint on how to implement methods and the development of additional, less-applicable, and more successful hybridization techniques.

2. EXPERIMENTAL SETUP

2.1. Modeling of PV-based DG systems considering islanding

Usually, a PV-based DG unit consists of a PV solar array, a DC-AC PV inverter, a parallel *RLC* load and a switch like a circuit-breaker or a fuse. Islanding operation of a PV-based DG unit can be produced when a part of the electric grid is disconnected to the main power grid while the nearby DG unit still powers it. Figure 1 and Figure 2 [18] depicts a PV-based DG system in normal and islanding operation modes, respectively. Next, the main components of the studied PV system are presented.

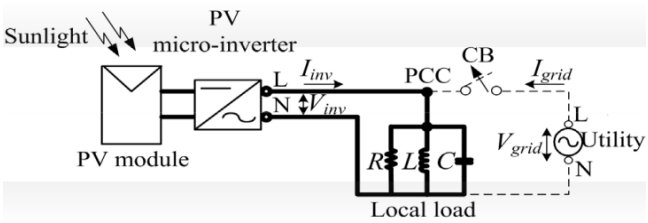

Fig. 1. Single PV inverter system in grid-connected configuration [18].

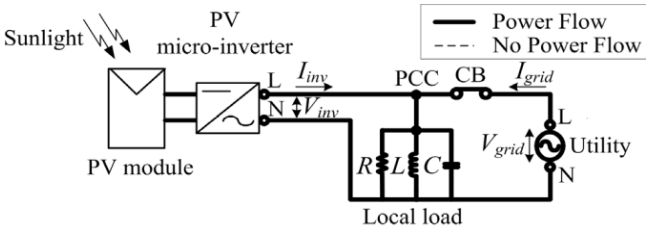

Fig. 2. Single PV inverter system configuration with islanding phenomenon mode [18].

2.1.1. DC-AC inverter

The single-phase full-bridge DC-AC inverter [19] converts the 400 V DC output voltage into 240 V AC at 60 Hz grid frequency.

2.1.2. Control strategy

The control system contains: a MPPT controller, a DC voltage regulator, a current regulator, a phase-locked loop (PLL) unit for grid synchronization, a PWM modulator, and the anti-islanding detection unit with studied active methods which disconnect the PV inverter using passive UOV/UOF relays. The MPPT extract the maximum power from a PV system in various weather conditions [17].

2.1.3. Sandia frequency shift method

The SFS method improves the performance of the active frequency drift technique by adding positive feedback to drift faster the frequency away from the nominal grid frequency. Consequently, the NDZ of the SFS method is significantly reduced. The SFS inverter current is expressed by [15, 20]:

$$I_{SFS} = \sqrt{2} I \sin\left[2\pi f t + \theta_{SFS}\right] \tag{1}$$

where I is the PCC current, f is the PCC frequency, t is the time, and θ_{SFS} is the phase angle of SFS method. The phase angle θ_{SFS} for SFS method is expressed by [20]:

$$\theta_{SFS} = \frac{c_{f_0} + k\left(f - f_g\right)}{2} \tag{2}$$

where c_{f_0} represents the initial chopping factor, k is a positive feedback gain which allows adjusting the islanding detection time, and f_g is the nominal frequency of the grid (60 Hz). The chopping factor c_f is varied according to the measured frequency drift [15]:

$$c_f = c_{f_0} + k\left(f - f_g\right) \tag{3}$$

2.1.3. Slip mode phase shift method

The SMS method changes the inverter phase angle current with the variation of measured frequency with respect to the nominal grid frequency [20]. The phase angle is given by [7]:

$$\theta_{SMS} = \frac{2\pi}{360}\theta_m \sin\left(\frac{\pi}{2}\frac{f - f_0}{f_m - f_0}\right) \tag{4}$$

where f_m is the frequency when θ_m increase and f_m - f_0 = 3 Hz [16]. The SMS inverter current is [7]:

$$I_{SMS} = \sqrt{2} I \sin\left[2\pi f t + \theta_{SMS}\right] \tag{5}$$

To cover islanding, a typical load curve of a PV inverter as in Figure 3 is considered. The shape of the frequency phase curve in Figure 3 for the interval of 59.3 – 60.5 Hz is sinusoidal and the load line represented as a parallel

RLC load has a negative slope. In the grid-connected mode, the current phase is determined by the grid frequency without taking into account the load line [7]. When an islanding situation happens, the frequency movement is different up or down to the zero point which is situated in the intersection of load line and SMS line in Figure 3 [7]. This islanding condition is happened when [15]:

$$\left.\frac{d\theta_{load}}{df}\right|_{f=f_g} \leq \left.\frac{d\theta_{SMS}}{df}\right|_{f=f_g} \tag{6}$$

where θ_{load} is the load phase angle. From [7] and [15] it results:

$$\theta_m \geq \frac{12Q_f}{\pi^2}\left(f_m - f_g\right) \tag{7}$$

If the PCC frequency decreases after the grid interruption, then it continuously decreases until it is sensed by the under frequency relay [7].

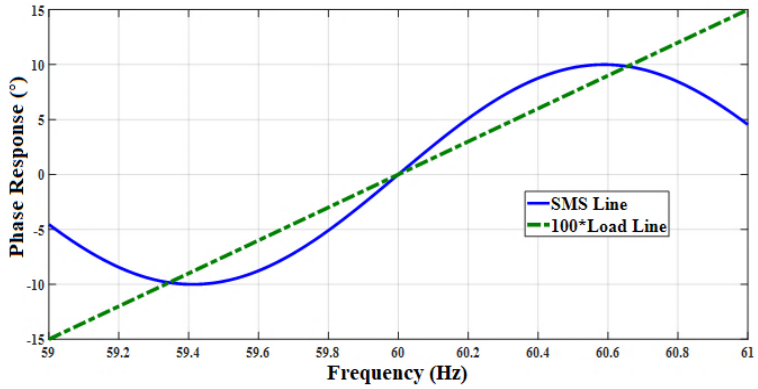

Fig. 3. SMS line and local load line.

2.1.3. Passive disconnection relay concept

The islanding detection algorithm works on the principle of UOV and UOF prevention after that the islanding is detected by the used active methods. The NDZ principle of the passive techniques is illustrated in Figure 4. V_{min}, V_{max}, f_{min}, and f_{max} are the UOV and UOF boundaries.

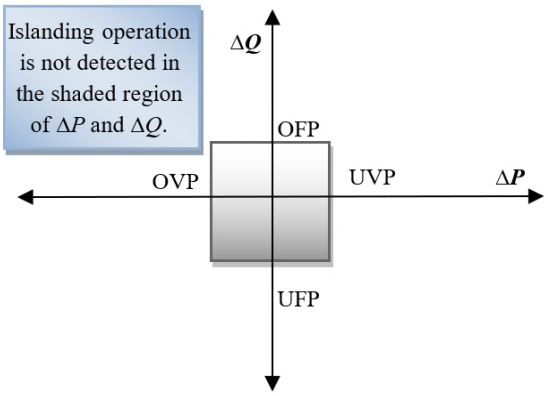

Fig. 4. NDZ for UOV and UOF passive techniques: UVP—under voltage protection; OVP—over voltage protection; UFP—under frequency protection; OFP—over frequency protection.

2.2. Modeling of PV-based DG systems considering islanding

A model of PV inverter using the SFS and SMS anti-islanding methods is developed under the Matlab/Simulink environment and shown in Figure 5. Figure 5 depicts the block diagram of the studied single-phase transformerless grid-connected PV system developed based on the model from [21], which consists of a 3.5-kW

PV array, a PWM-controlled single-phase DC-AC converter (inverter) with P&O MPPT method and injected by current of anti-islanding method, a block to measure the voltage and the frequency which normally generates a fault signal to disconnect the PV inverter based on the UOV and UOF passive methods, and a *LCL* grid-side filter. In this paper, the exact time of disconnection is given by an independent Clock block, which allows the comparison between each islanding PV inverter disconnection time. The parameters of the proposed grid-connected PV system are specified in Table 1.

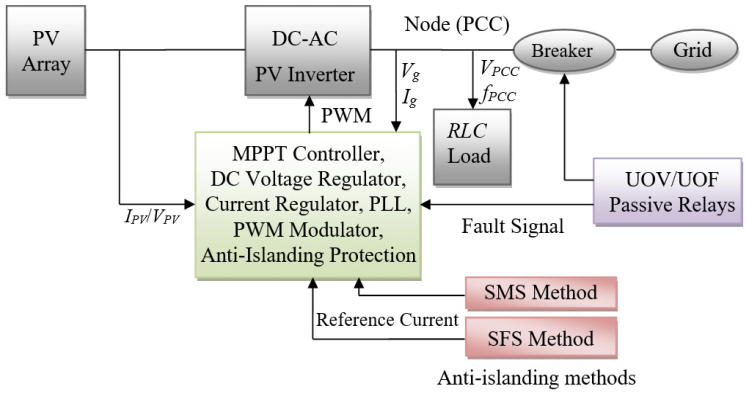

Fig. 5. Block diagram of the single-phase grid-connected PV system applying the studied anti-islanding methods.

The passive methods are realized as in [22]. Figure 6 and Figure 7 illustrate the implemented models in Simulink of the SFS and SMS active methods which are published in the literature as stated above.

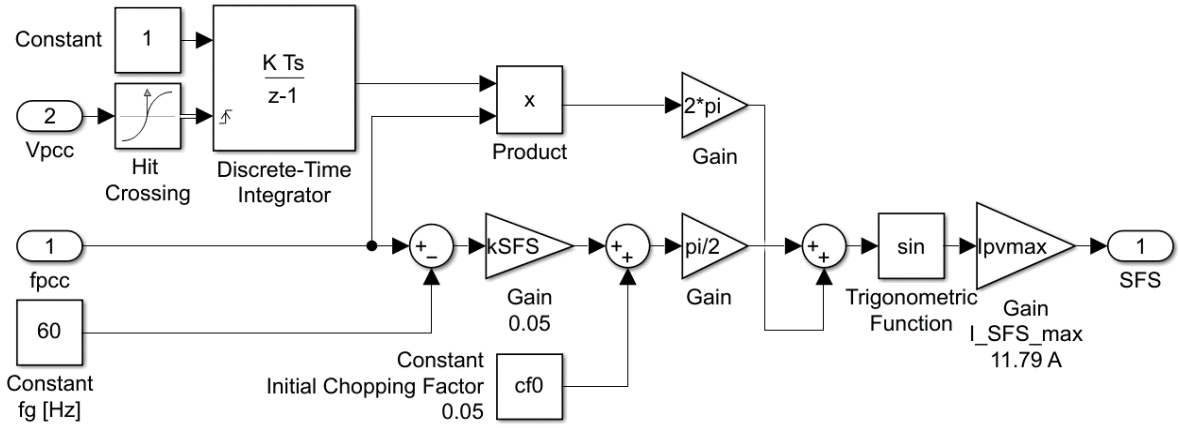

Fig. 6. Simulink block of SFS method.

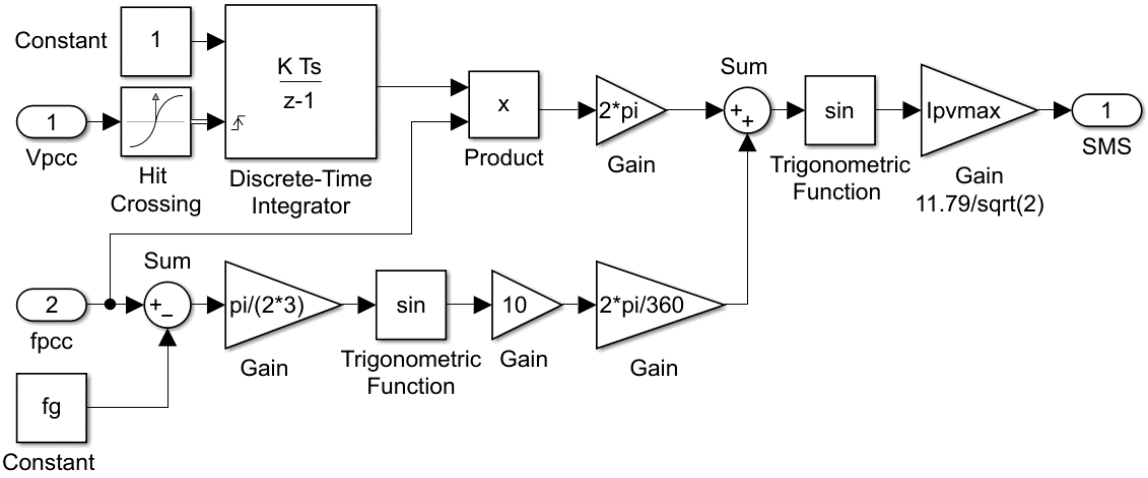

Fig. 7. Simulink block of SMS method.

Table 1. System parameters in compliance with the IEEE Std. 929

Parameter		Values
Nominal line frequency (f_g) [Hz]		60
Grid voltage (V_g) [V]		240
f_{min}/f_{max} [Hz]		59.3/60.5
V_{min}/V_{max} [V]		211.2/264
DG output power [kW]		3.5
Input DC voltage [V]		434
Grid side inductor of the *LCL* grid filter [mH]		1.73
PV inverter side inductor of the *LCL* grid filter [μH]		12
Capacitor of the *LCL* grid filter [μF]		15
RLC Load	Active power (P) [kW]	3.5
	Inductive reactive power (positive var): (Q_l) [kVar]	8.750
	Capacitive reactive power/negative var: (Q_c) [kVar]	8.750
Quality factor (Q_f)		2.5

3. SIMULATION RESULTS AND DISCUSSION

3.1. Influence of the non-detection zone

The NDZ for each method is determined by frequency as a function of Q_f. Figure 8 and Figure 9 presents exactly the NDZ of the studied system with SMS and SFS methods and their different parameters in the f - Q_f curve and with UFP/OFP limits (f = 60.5 Hz/f = 59.3 Hz), respectively. The steady state frequency of the island DG system will be out of the limits of the frequency relays according to the previous equations and the inverter will be then tripped. The intersections of the obtained curves with the UFP/OFP lines form the NDZ of each method.

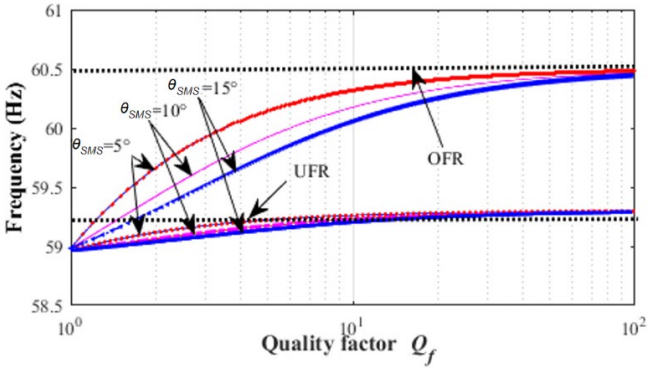

Fig. 8. NDZ of the SMS method.

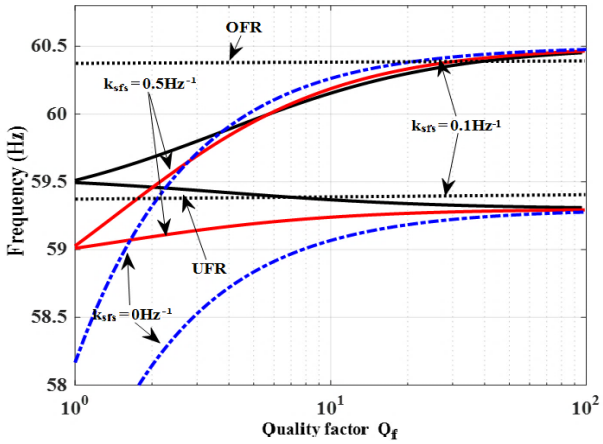

Fig. 9. NDZ of the SFS method.

The studied methods have different NDZ. However, the SMS and SFS methods have the same NDZ for Q_f equal to or greater than 10. For the Q_f less than this value the specific parameters of each method (phase angle θ_{SMS} for SMS and c_f and c_{f_0} for SFS) give much interaction.

3.2. Influence of the quality factor

The quality factor Q_f for a parallel *RLC* load is the ratio between the stored energy and dissipated energy per cycle for a given frequency [1, 15]. Figure 10 presents the load phase angle θ_{load} versus frequency curves for loads with different Q_f and resonant frequencies f_0 for a parallel *RLC* load. As can be observed in Figure 10, the load impedance varies for different frequencies. Figure 11 presents the current-voltage phase-angle of the load versus frequency f and different Q_f and resonant frequencies f_0. It can be seen from Figure 11 that for large values of Q_f the load resonant frequency has more effect on phase load output. The obtained results presented in Figure 10 and Figure 11 contribute to the performance of the grid-connected PV system. Note that the Q_f in the figures is given by logarithmic scale.

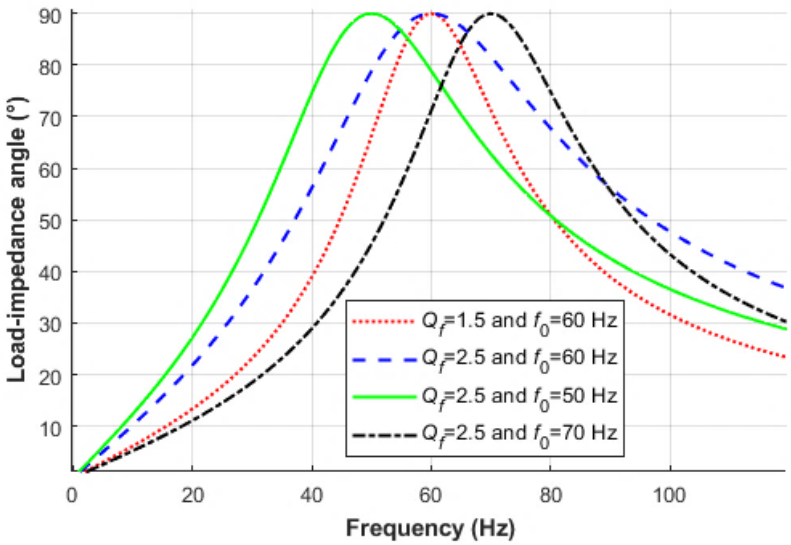

Fig. 10. Load-impedance phase-angle versus grid frequency.

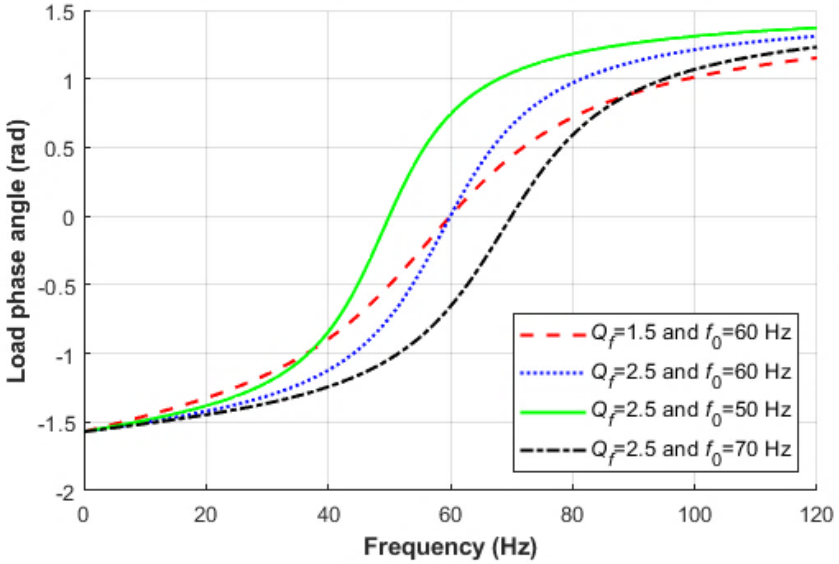

Fig. 11. Load current voltage phase-angle versus grid frequency.

The influence of Q_f is bigger for the small value less than 10 and NDZ forms changed in relation to their essential parameters. However, for greater values of Q_f than 10, the Q_f influence is the same for both methods.

3.3. Comparative simulation results

More simulation tests are carried out using the developed PV system model in Matlab/Simulink according to the electrical schematic from Figure 5. The islanding mode is marked at $t = 0.5$ s. The NDZ of each method has been evaluated considering 0.88 p.u. to 1.1 p.u. and 59.3 Hz to 60.5 Hz as limits for UOV/UOF blocks and $Q_f = 2.5$. The SFS method has been considered for three cases of K_{SFS}: 0 Hz^{-1}, 0.1 Hz^{-1}, and 0.5 Hz^{-1}. In the case of the SMS method, three values of θ_m have been considered (5°, 10°, and 25°), where the *RLC* load values are presented in Table 1.

According to the IEEE Std. 929, the grid breaker opens after 6 cycles from the beginning to ensure the island mode [15]. In this study, the fault signal is not connected to the circuit breaker of the PV inverter to disconnect it after islanding detection and the PV system continues to supply the grid to show how the main grid parameters vary in PCC after islanding.

3.3.1. SFS method results

Figure 12 shows the voltage, current, active power, and reactive power variations of the SFS anti-islanding method and for varied values of K_{SFS} (0 Hz^{-1}, 0.1 Hz^{-1}, and 0.5 Hz^{-1}). Figure 13 also presents the frequency variation with the same parameters.

The largest islanding detection time was $t = 181.57$ ms in the case of $K_{SFS} = 0$ Hz^{-1}. The smallest detection time was obtained in the case of $K_{SFS} = 0.1$ Hz^{-1} ($t = 75.1$ ms). Moreover, the PV power inverter loses its stability after the frequency point of islanding detection for all chosen values of K_{SFS} parameter and the islanding mode is quickly detected.

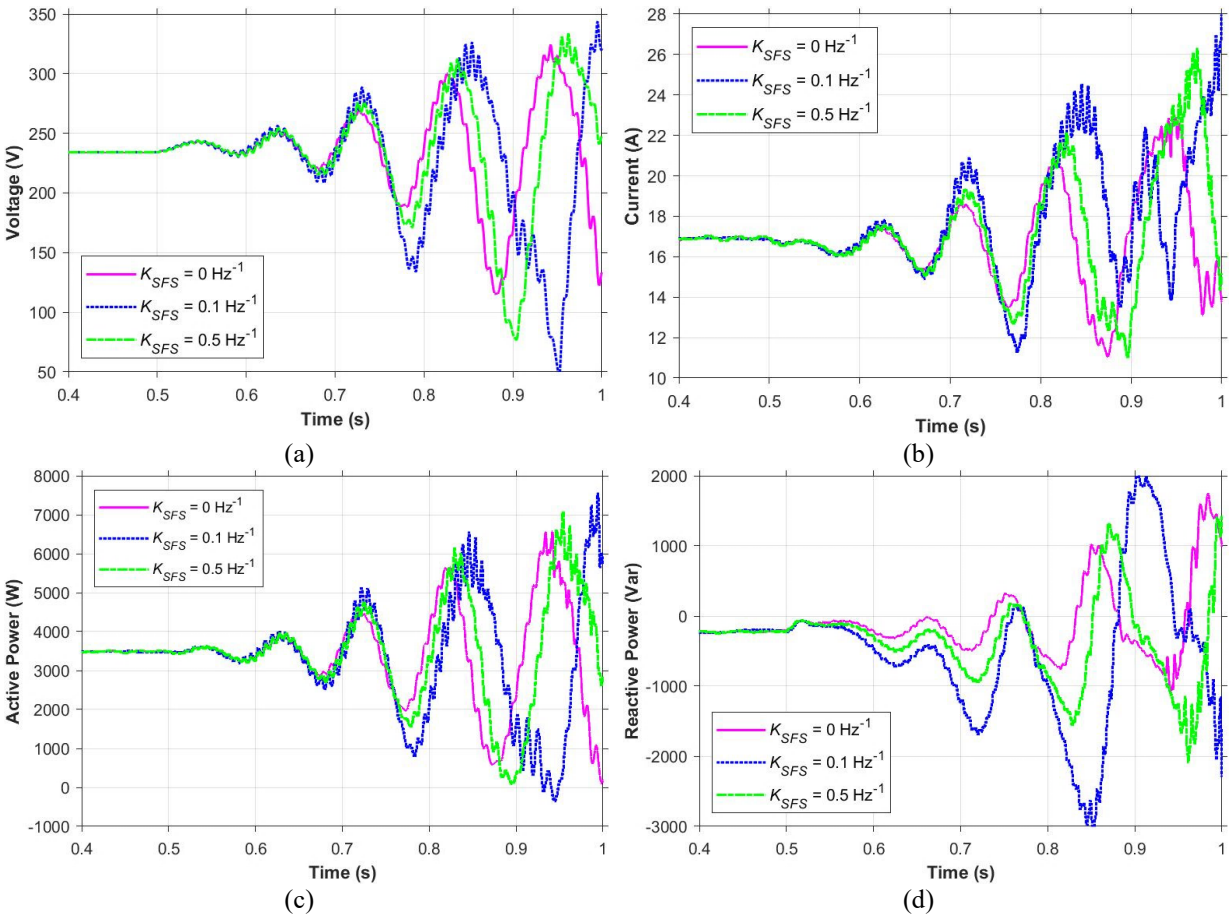

Fig. 12. Islanding test for SFS method with different values of K_{SFS} parameter. (a) PCC voltage. (b) PCC current. (c) Active power. (d) Reactive power.

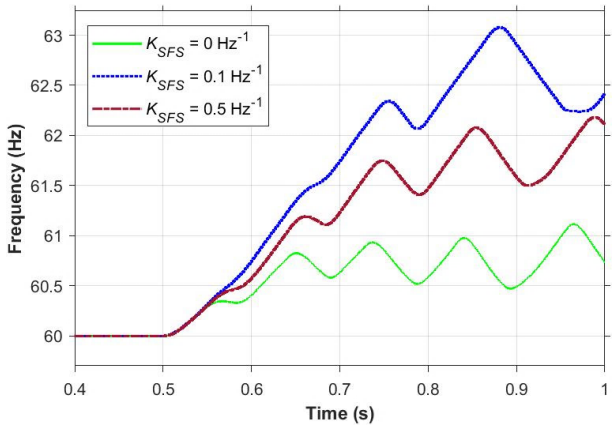

Fig. 13. Frequency variation waveforms in the case of an islanding test for SFS method with different values of K_{SFS}.

3.3.2. SMS method results

Similar islanding tests were performed for the grid-connected PV system with SMS method and different values for θ_m (5°, 10°, and 25°). Figure 14 show the system response with SMS method: V_{PCC} voltage, I_{PV} current, active power, and reactive power for different θ_m values under the same conditions of the SFS methods, while Figure 15 shows the frequency response of the PV system with SMS method under the same variations of θ_m parameter. The breaker is opened at t = 0.5 s. The best condition is obtained for θ_m = 25° (islanding detection time t = 152.4 ms). It is noted that for θ_m = 5° and θ_m = 10°, the voltage frequency f_{PCC} decreased and became lower than the UFP set point after the grid disconnection. The frequency exceeds the lower limits of frequency at 273 ms and 314.8 ms, respectively. These islanding detection times are very slow compared to the θ_m =25° case.

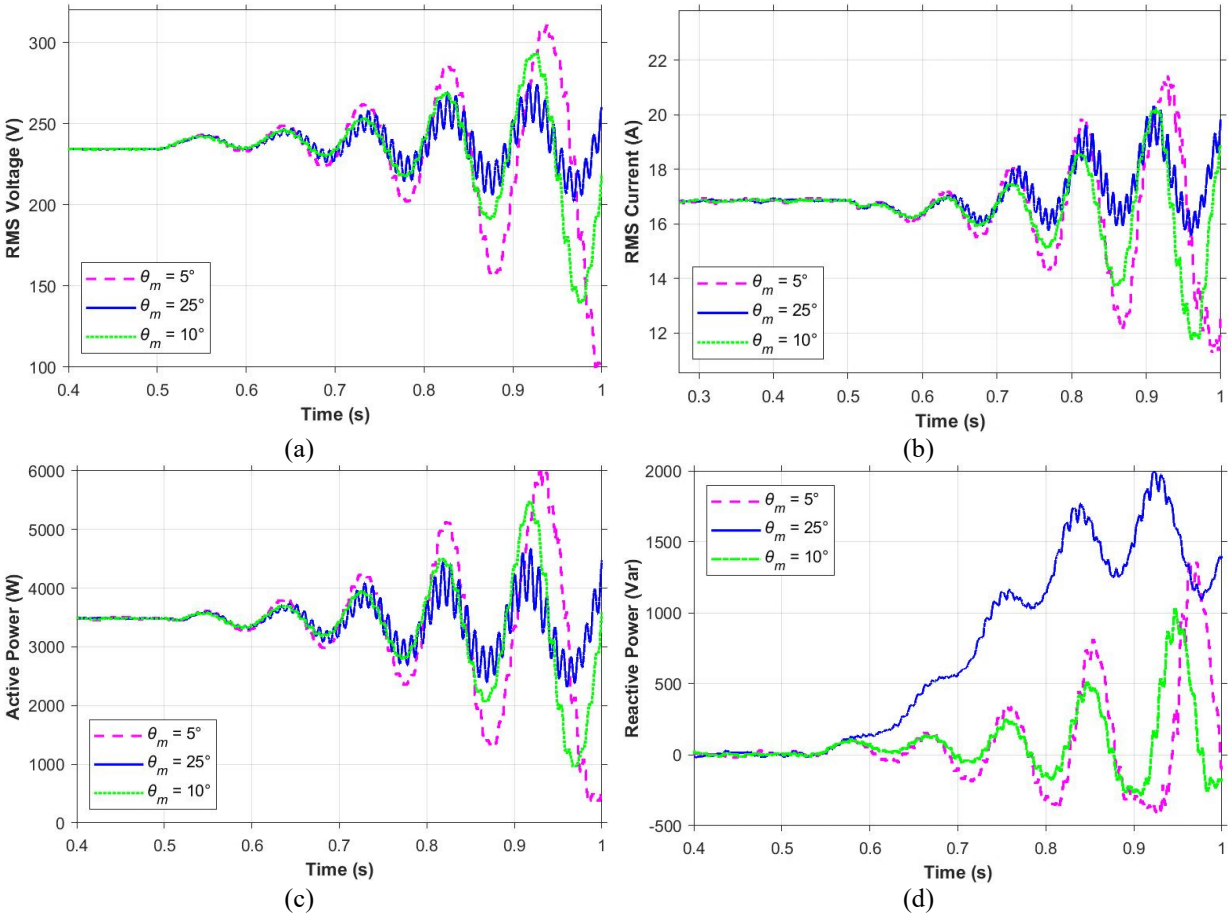

Fig. 14. Islanding test for SMS method with different values of parameter: (a) PCC voltage; (b) PCC current; (c) Active power variation; (d) Reactive power variation.

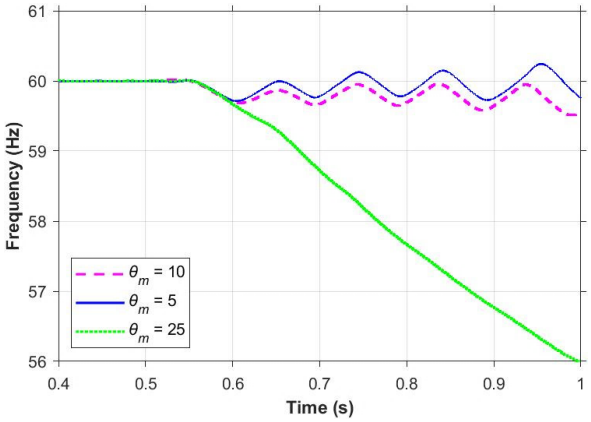

Fig. 15. PCC frequency waveform in case of an islanding test for SMS method with different θ_m values.

According to the IEEE Std. 929 (f_m - f_g = 3 Hz), the worst case occurs when the load has Q_f = 2.5, which is not verified for θ_m = 5 and verified when θ_m = 25° and θ_m = 10°; that prove the simulation results in this work.

The obtained results are presented in Table 2. The essential parameters of the studied active anti-islanding methods have been varied within the 2 s required by the IEEE Std. 929 and IEEE Std. 1547.1 [23].

Table 2. Simulation results

Active anti-islanding method	Parameters	Detection time	Islanding detection state
SFS	K_{SFS} = 0 Hz^{-1}	111.6 ms	work
	K_{SFS} = 0.1 Hz^{-1}	75.1 ms	work
	K_{SFS} = 0.5 Hz^{-1}	91. ms	work
SMS	θ_m = 5°	273 ms	work
	θ_m = 10°	314.8 ms	work
	θ_m = 25°	152.4 ms	work

In order to select the right parameters for each technique, it is intended to demonstrate that the parameters and the methods under study interact. This study shows that the anti-islanding methods employed have a substantial correlation with their self-parameters (c_f in the case of SFS and θ_m in the case of SMS).

4. CONCLUSIONS

This paper compared two active islanding techniques, the SMS and SFS methods. These techniques have demonstrated their impact on islanding detection, in a proposed system composed of a single-phase transformerless grid-connected PV system. Each approach is unique has benefits and disadvantages. They have certain limitations that can be improved using the hybridization technique with other passive methods which give different interactions with voltage, current, frequency, or even active and reactive power. The relationship between under/over current, voltage, and frequency is demonstrated to be distinct. The hybridization with passive methods can open a new horizon in the improvement of methods. It is recommended to use both methods in the case of a multi inverter system to benefit from both methods' advantages as in [9].

The following conclusions can be made in the light of the preceding results:

- The simulation results of these islanding detection methods have been mapped to compare between them and to compare the same method with their parameters to verify their compatibility with the system, which is a PV system with PWM controlled single-stage PV inverter and MPPT controller.
- Mathematical proofs and the results obtained confirm the performance of the studied anti-islanding methods under varying parameters for frequency, local load, and for the methods themselves.
- The NDZ for each method is also highlighted for different cases where satisfactory results are obtained.

- There is a small deviation in the islanding detection time of each method, which does not exceed the condition of 2 s required by the IEEE Std. 929 and IEEE Std. 1547.1 for successful detection. This proves the performance and effectiveness of these active methods. In case of failure in detection, this small deviation in islanding detection can highlight the limits of the applied methods.
- The results show that SMS and SFS methods provide good islanding detection. The SFS method requires an active power change greater than the reactive power change required by the SMS method. Therefore, if it is not possible to implement both methods at the same time, it is recommended to implement the SMS method.
- This study can be considered as bibliography for further research. Future investigations can include experimental research and studies using multiple PV inverters configurations in both cases simulation and experimentation.

Data Availability Statement: *The authors confirm that the data supporting the findings of this study are available within the article*

Acknowledgments: *This work was supported by VILLUM FONDEN under the VILLUM Investigator Grant (no. 25920): Center for Research on Microgrids (CROM); www.crom.et.aau.dk*

Conflicts of Interest*: The authors declare no conflicts of interest.*

REFERENCES

[1] IEEE Recommended practice for utility interface of photovoltaic (PV) systems, IEEE Std. 929-2000.
[2] Arulkumar, K., Vijayakumar, D., Palanisamy, K., Recent advances and control techniques in grid connected PV system–A review, International Journal of Renewable Energy Research, vol. 6, no. 3, 2016, pp. 1037-1049.
[3] Yu, B., Matsui, M., Yu, G., A review of current anti-islanding methods for photovoltaic power system, Solar Energy, vol. 84, no. 5, 2010, pp. 745-754.
[4] Teodorescu, R., Liserre, M., Rodriguez, P., Grid converters for photovoltaic and wind power systems, John Wiley and Sons, Ltd., Chichester, 2011.
[5] Ye, Z., Kolwalkar, A., Zhang, Y., Du, P., Walling, R., Evaluation of anti-islanding schemes based on nondetection zone concept, IEEE Transactions on Power Electronics, vol. 19, no. 5, 2004, pp. 1171-1176.
[6] Wang, X., Freitas, W., Xu, W., Dynamic non-detection zones of positive feedback anti-islanding methods for inverter-based distributed generators, IEEE Transactions on Power Delivery, vol. 26, no. 2, 2011, pp. 1145-1155.
[7] Yu, B., Matsui, M., Jung, Y., Yu, G., Modeling and design of phase shift anti-islanding method using non-detection zone, Solar Energy, vol. 81, no. 11, 2007, pp. 1333-1339.
[8] Kong, X., Xu, X., Yan, Z., Chen, S., Yang, H., Han, D., Deep learning hybrid method for islanding detection in distributed generation, Applied Energy, vol. 210, 2018, pp. 776-785.
[9] Barkat, F., Cheknane, A., Guerrero, J.M., Lashab, A., Istrate, M., Banu, I.V., Hybrid islanding detection technique for single-phase grid-connected photovoltaic multi-inverter systems, IET Renewable Power Generation, vol. 14, no. 18, 2020, pp. 3864-3880.
[10] Seyedi, M., Taher, S.A., Ganji, B., Guerrero, J.M., A hybrid islanding detection method based on the rates of changes in voltage and active power for the multi-inverter systems, IEEE Transactions on Smart Grid, vol. 12, no. 4, 2021, pp. 2800-2811.
[11] Baghaee, H.R., Mlakić, D., Nikolovski, S., Dragicčvić, T., Anti-islanding protection of PV-based microgrids consisting of PHEVs using SVMs, IEEE Transactions on Smart Grid, vol. 11, no. 1, 2020, pp. 483-500.
[12] Worku, M.Y., Hassan, M.A., Maraaba, L.S., Abido, M.A., Islanding detection methods for microgrids: a comprehensive review, Mathematics, vol. 9, no. 24, 2021, pp. 3174-3196.
[13] Khosravi, H., Samet, H., Tajdinian, M., Robust Islanding detection in microgrids employing rate of change of kinetic energy over reactive power, IEEE Transactions on Smart Grid, vol. 13, no. 1, 2022, pp. 505-515.
[14] Fathi-Jowzdani, A.H., Sadeghkhani, I., Mehrizi-Sani, A., Islanding detection for DC microgrids based on episode of care severity index, IEEE Transactions on Smart Grid, vol. 13, no. 2, 2022, pp. 954-961.
[15] Lopes, L.A., Sun, H., Performance assessment of active frequency drifting islanding detection methods, IEEE Transactions on Energy Conversion, vol. 21, no. 1, 2006, pp. 171-180.
[16] Xu, M., Melnik, R.V., Borup, U., Modeling anti-islanding protection devices for photovoltaic systems, Renewable Energy, vol. 29, no. 15, 2004, pp. 2195-2216.

[17] Abdelsalam, A.K., Massoud, A.M., Ahmed, S., Enjeti, P.N., High-performance adaptive perturb and observe MPPT technique for photovoltaic-based microgrids, IEEE Transactions on Power Electronics, vol. 26, no. 4, 2011, pp. 1010-1021.
[18] Yu, B., An improved active frequency drift anti-islanding method for multiple PV micro-inverter systems, IEICE Electronics Express, vol. 11, no. 6, 2014, pp. 1-11.
[19] Ciobotaru, M., Teodorescu, R., Blaabjerg, F., Control of single-stage single-phase PV inverter, EPE Journal, vol. 16, no. 3, 2006, pp. 20-26.
[20] Estébanez, E.J., Moreno, V.M., Pigazo, A., Liserre, M., Performance evaluation of active islanding-detection algorithms in distributed-generation photovoltaic systems: Two inverters case, IEEE Transactions on Industrial Electronics, vol. 58, no. 4, 2011, pp. 1185-1193.
[21] MATLAB, 2022. Natick, Massachusetts: The MathWorks Inc. Single-Phase, 240 Vrms, 3500 W Transformerless Grid-Connected PV Array. Available online: https://www.mathworks.com/help/physmod/sps/ug/single-phase-240-vrms-3500-w-transformerless-grid-connected-pv-array.html (10.04.2022).
[22] Banu, I.V., Istrate, M., Machidon, D., Pantelimon, R., A study on anti-islanding detection algorithms for grid-tied photovoltaic systems, International Conference on Optimization of Electrical and Electronic Equipment (OPTIM), IEEE, Bran, Romania, 2014, pp. 655-660.
[23] Standard conformance test procedures for equipment interconnecting distributed energy resources with electric power systems and associated interfaces, IEEE Std. 1547.1-2020.